Springer

Journal of Mechanical Science and Technology 23 (2009) 2330~2340

Journal of Mechanical Science and Technology

www.springerlink.com/content/1738-494x
DOI 10.1007/s12206-009-0620-0

A study on the analysis of O-ring under uniform squeeze rate and internal pressure by photoelastic experimental hybrid method †

Jaisug Hawong[1,*], Jeonghwan Nam[1], Songling Han[2], Osung Kwon[2] and Sunghan Park[3]

[1]*School of mechanical Engineering, Yeungnam University, Gyeongsan, 712-749, Korea*
[2]*Gradute School, School of mechanical Engineering, Yeungnam University, Gyeongsan, 712-749, Korea*
[3]*Agency for Defense Development, Daejeon, Korea*

(Manuscript Received February 13, 2009; Revised April 9, 2009; Accepted May 27, 2009)

Abstract

There are three kinds of loading conditions applied to the O-ring, The first loading condition is the case in which uniform squeeze rates are applied to the upper side and the lower side of the O-ring (the strain condition). The second loading condition is the case in which uniform squeeze rates are applied to the upper side and the lower side of the O-ring and other squeeze rates are applied to the front side of the O-ring. The third loading condition is the case in which uniform squeeze rates are applied to the upper side and the lower side of the O-ring, other squeeze rates are applied to the front side of the O-ring, and internal pressures are applied to another front side of the O-ring(loading condition is the combination of stress condition and the strain condition). In this research, a new photoelastic experimental hybrid method under the third loading condition was developed and it was verified. The stresses of the O-ring under the third loading condition were analyzed by the new photoelastic experimental hybrid method developed in this research. The internal pressures applied to the O-ring were 0.98 MPa, 1.96 MPa, 2.94 MPa and 3.92 MPa.

Keywords: Hook-Jeeves' numerical method; Internal pressure; Isochromatic fringe pattern; Photoelastic experimental hybrid method; Stress optic law; Stress freezing cycle; Squeeze rate

1. Introduction

Rubber O-ring have been used as a packing element for high pressure vessels, oil-pressure parts, airplane parts and nuclear generator parts etc. There are three kinds of loading conditions applied to the O-ring: first, uniform squeeze rates are applied to the upper side and the lower side of the O-ring (the strain condition); second is the case in which uniform squeeze rates are applied to the upper side and the lower side of the O-ring and other squeeze rates are applied to the front side of the O-ring; and third, the case in which uniform squeeze rates are applied to the upper side and the lower side of the O-ring; other squeeze rates are applied to the front side of the O-ring, and internal pressures are applied to another front side of the O-ring(loading condition is the combination of stress condition and the strain condition).

The stresses of the O-ring have been analyzed for very complicated loading conditions [1-6]. In this study, the stresses of the O-ring under the first loading condition or the second loading condition were investigated [7]. The stresses of the O-ring under the third loading condition have not been studied. The photoelastic experimental hybrid method used until now has been applied in diverse ways in investigations of the internal traction free surface such as a circular hole and crack and the external traction free surface such as an O-ring under uniform squeeze rate. [8-13]

The stress of the O-ring under the third loading condition was analyzed by the new photoelastic experimental hybrid method developed in this research

† This paper was recommended for publication in revised form by Associate Editor Jooho Choi
*Corresponding author. Tel.: +82 53 8102445, Fax.: +82 53 810 4627
E-mail address: jshawong@ynu.ac.kr

using the relationships between two stress functions for contact stress problems. The main purpose of this study is to develop a new photoelastic experimental hybrid method to apply in the stress analysis of the O-ring under the third loading condition. The detailed aims of this research are as follows;

(1) Validation of the new photoelastic experimental hybrid method.
(2) Stress analysis of the contact stress of the O-ring under the third loading condition.
(3) Stress analysis of the internal stress of the O-ring under the third loading condition.
(4) The relationships between the internal stress of the O-ring and the internal pressure and between the contact stress of the O-ring and the internal pressure.

2. Basic theory

2.1 Stress components

Eq. (1) gives the stress components using Muskhelishvili complex function [14] and Airy stress function [15].

$$\begin{aligned}\sigma_x &= \mathrm{Re}\left[2\phi'(z) - \bar{z}\phi''(z) - \Psi'(z)\right]\\ \sigma_y &= \mathrm{Re}\left[2\phi'(z) + \bar{z}\phi''(z) + \Psi'(z)\right]\\ \tau_{xy} &= \mathrm{Im}\left[\bar{z}\phi''(z) + \Psi'(z)\right]\end{aligned} \tag{1}$$

Where z=x+iy,

Re(Im): real(imaginary) part of complex.

As shown in Eq. (1), the stress components are composed of two complex functions. Therefore, for any case, if two stress functions are known, the stress components are determined.

In general, the relative equations between two stress functions are determined from the traction free condition on the free surface. The photoelastic experimental hybrid method using the internal traction free condition or external traction free condition has been already developed. [7, 8, 11] The loading condition of this study is the restrain condition for the contact between the O-ring and cylinder as shown in Fig. 1.

As shown in Fig. 1, the relative equation between two stress functions is not determined from the internal traction free condition or external traction-free condition on the loading condition in Fig. 1. The loading condition of Fig. 1 is a contact problem.

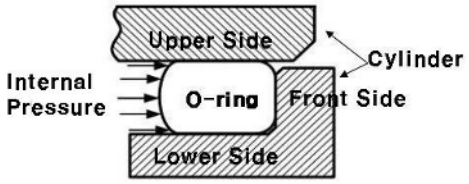

Fig. 1. Restraint condition for the contact between the O-ring and cylinder.

In general, a contact problem is a half-plane problem. If a structure belongs to the upper half plane (z > 0), the stress component equations and complex variables belong to the half plane. Therefore, a complex variable ϕ (z) in the lower half plane (z < 0) is defined as Eq. (2a) [16].

$$\phi(\bar{z}) = -\overline{\phi(z)} - \bar{z}\overline{\phi'(z)} - \overline{\Psi(z)} \tag{2a}$$

$$\Psi(z) = -\phi(z) - \overline{\phi(\bar{z})} - z\phi'(z) \tag{2b}$$

Conjugating both sides of Eq. (2a) and rearranging the equation, the complex variable Ψ (z) of the lower half plane can be expressed by Eq. (2b).

Eq. (2b) is very important because it indicates the relative equation between the stress function ϕ (z) and stress function Ψ (z).

Substituting Eq. (2b) for Eq. (1), Eq. (3) is obtained in terms of only one stress function ϕ (z).

$$\begin{aligned}\sigma_x &= \mathrm{Re}\left[3\phi(z) + \overline{\phi(\bar{z})} + z\phi'(z) - \bar{z}\phi'(z)\right]\\ \sigma_y &= \mathrm{Re}\left[\phi(z) - \overline{\phi(\bar{z})} - z\phi'(z) + \bar{z}\phi'(z)\right]\\ \tau_{xy} &= \mathrm{Im}\left[-\phi(z) - \overline{\phi(\bar{z})} - z\phi'(z) + \bar{z}\phi'(z)\right]\end{aligned} \tag{3}$$

As shown in Eq. (3), if only complex function ϕ (z) is determined, the stress components can be determined. Because stress functions ϕ (z) and ϕ (z) are analytic functions, ϕ (z) and Ψ (z) can be expressed by a power series by Eq. (4).

$$\phi(z) = \sum_{n=0}^{N} C_n z^{\frac{n}{2}}, \quad \Psi(z) = \sum_{n=0}^{N} D_n z^{\frac{n}{2}} \tag{4}$$

Substituting Eq. (4) for Eq. (2b), the relative equation between the coefficients of two stress functions ϕ (z) and Ψ (z) is obtained by Eq. (5).

$$D_n = -\frac{n}{2}C_n - \overline{C_n} \tag{5}$$

Using two stress functions ϕ(z), Ψ(z) and the relative equation between the coefficients of two stress functions ϕ(z) and Ψ(z), stress components are obtained as Eq. (6).

$$\begin{aligned}\sigma_x(z) &= \sum_{n=1}^{N} \mathrm{Re}\begin{Bmatrix} C_n\left[2F(n,z)-G(n,z)\right] \\ +\bar{C}_n F(n,z)\end{Bmatrix} \\ \sigma_y(z) &= \sum_{n=1}^{N} \mathrm{Re}\begin{Bmatrix} C_n\left[2F(n,z)+G(n,z)\right] \\ -\bar{C}_n F(n,z)\end{Bmatrix} \\ \tau_{xy}(z) &= \sum_{n=1}^{N} \mathrm{Im}\left\{C_n G(n,z)-\bar{C}_n F(n,z)\right\}\end{aligned} \tag{6}$$

where $F(n\cdot z)=\frac{n}{2}z^{\frac{n}{2}-1}$

$$G(n\cdot z)=\frac{n}{2}\left\{\left(\frac{n}{2}-1\right)\bar{z}-\frac{n}{2}z\right\}z^{\frac{n}{2}-2}$$

2.2 New photoelastic experimental hybrid method

Eq. (7a) is the stress optic law [17] for an isotropic material.

$$\left(\frac{f_\sigma \cdot N_f}{t}\right)^2 = \left(\sigma_x-\sigma_y\right)^2+\left(2\tau_{xy}\right)^2 \tag{7a}$$

$$\begin{aligned}&\left(\frac{f_\sigma \cdot N_f}{t}\right)^2-\left(\sigma_x-\sigma_y\right)^2-\left(2\tau_{xy}\right)^2 \\ &= D(\varepsilon)\end{aligned} \tag{7b}$$

Substituting the stress fringe value f_σ, isochromatic fringe order N_f, specimen thickness t and position coordinates z etc. for Eq. (7a), Eq. (7a) becomes a function of only coefficients a_n and b_n of a complex variable, that is, a function of only $c_n = a_n + ib_n$. Substituting precise experimental data for Eq. (7a), errors are generated, as given by Eq. (7b). Therefore, the error function $D(\varepsilon)$ cannot be zero.

Therefore, we should use the numerical method to minimize the errors. The converging conditions used in this research are $D(\varepsilon) \le 10^{-5}$

If $D(\varepsilon) \le 10^{-5}$, errors almost converge to zero.

Substituting Eq. (6) for Eq. (7b), Eq. (8) is obtained.

Substituting the measured fringe order (N_f), measured position of fringe order ($z = x + iy$), thickness of specimen (t) and stress fringe values (f_σ) for Eq. (8), Eq. (8) becomes a function of only $C_n (= a_n + ib_n)$.

Applying the numerical method to the Eq. (8) with the measured experimental data.

a_n and b_n are determined, which satisfies the limit values of errors.

Substituting $C_n (= a_n + ib_n)$ for Eqs. (5) and (4), stress functions ϕ(z) and $\psi(z)$ for the given conditions are determined.

Substituting the determined stress functions ϕ(z) and $\psi(z)$ for Eq. (1), the stress components of the structure under arbitrary load are determined. These procedures comprise the new photoelastic experimental hybrid method in this paper, in particular, the photoelastic experimental hybrid method for contact stress analysis.

$$\begin{aligned}D(\varepsilon) &= \left(\frac{f_\sigma \cdot N_f}{t}\right)^2-\left(\sigma_x-\sigma_y\right)^2-\left(2\tau_{xy}\right)^2 \\ &= \left(\frac{f_\sigma \cdot N_f}{t}\right)^2-\left\{\sum_{n=1}^{N} a_n \mathrm{Re}\left[2F(n,z)-2G(n,z)\right]\right. \\ &\quad \left.+\sum_{n=1}^{N} b_n \mathrm{Im}\left[2F(n,z)+2G(n,z)\right]\right\}^2 \\ &\quad -\left\{\sum_{n=1}^{N} a_n \mathrm{Im}\left[2G(n,z)-2F(n,z)\right]\right. \\ &\quad \left.+\sum_{n=1}^{N} b_n \mathrm{Re}\left[2F(n,z)+2G(n,z)\right]\right\}^2\end{aligned} \tag{8}$$

For the contact problems of two cylinders with an internal pressure, a traction free surface almost not exists on the cross-section of the cylinder. Therefore, the new photoelastic experimental hybrid method using the relative equation between two stress functions $\phi(z)$ and $\Psi(z)$ is effectively used to analyze stress of a cylinder (O-ring).

3. Experiment and experimental method

3.1 Specimen

To study the contact stress of the O-ring by the photoelastic experiment, an O-ring model should be made of polymer, which has photoelastic properties.

In this research, an epoxy resin was used as the model material. The cross-sectional diameter of the O-ring is 6.98 ± 0.15 *mm*, and the internal diameter of the O-ring is 121.5 ± 0.94 *mm*. The photoelastic material used in this research is epoxy resin, which is made from Araldite and hardener (Ciba-Geigy Co., weight ratio: 10:3).

In this research, we used molding procedures of the O-ring, and loading device developed by the authors[18]. We used the photoelastic experimental procedures on obtaining isochromatic fringe pattern used by the authors [18].

When the internal pressures 0.98 MPa, 1.96 MPa, 2.94 MPa and 3.92 MPa were respectively applied to the O-ring under 20% squeeze rate, the O-ring under 20% squeeze rate and the internal pressure was respectively frozen according to the stress freezing cycle.

3.2 photoelastic experimental hybrid method for stress analysis of the O-ring

The process of the photoelastic experimental hybrid method for stress analysis of the O-ring is as follows:

(1) Measure the mechanical properties, elastic modulus ($=E$) , Poisson's ratio ($=v$) and stress fringe values ($=f_\sigma$) .
(2) Magnify the isochromatic fringe patterns of each slice and record them in the personal computer with a digital camera.
(3) Measure 350~400 experimental data on the fringe orders of 0.5 times for squeeze rates of 20%, respectively.
(4) Substitute the measured experimental data for the stress optic law and apply the Hook and Jeeves' numerical method [19] to the stress optic law with the experimental data. C_n is calculated (n=14~16). When C_n is determined, $F(n,z)$ and $G(n,z)$ should be used in accordance with the procedures of the photoelastic experimental hybrid method. A stress function is obtained and another stress function is obtained from the relative equation of the two stress functions. Stress components are obtained by using Eq. (1) andtwo stress functions.
(5) Substitute the stress components obtainedabove for the stress optic law and plot the isochromatic. Compare the actual isochromaticwith the graphing isochromatic. When the graphing isochromatic is almost identical to the actual isochromatic, go to the next procedure. If the graphing isochromatic is notsimilar to the actual isochromatic, repeat the above processes until the graphing isochromatic is almost identical to the actual isochromatic.
(6) When the graphing isochromatic is identical to the actual isochromatic, stress functions are determined. Contact stresses andinternal stresses of the O-ring are determined. Plot the stress contour of the stress components normalized by the maximum contact pressure.

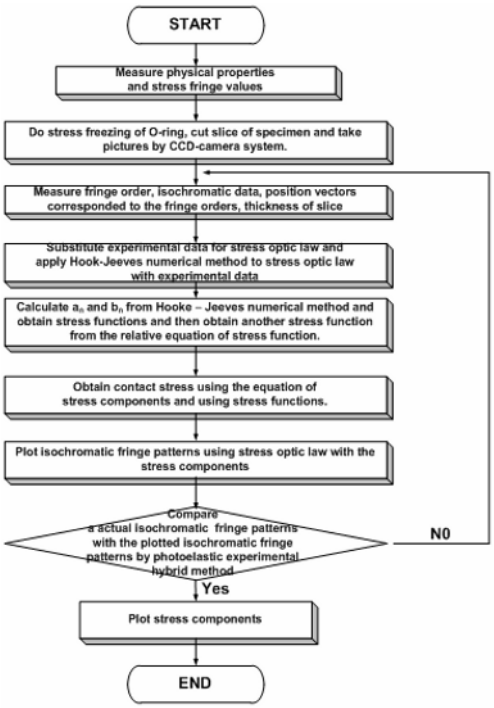

Fig. 2. Flow chart of new photoelastic experimental hybrid method for contact problem of O-ring.

Fig. 2 shows the flow chart of photoelastic experimental hybrid method for contact problem of O-ring under uniform squeeze rate and internal pressure.

4. Experimental results and discussions

When the internal pressures 0.98 MPa, 1.96 MPa, 2.94 MPa and 3.92 MPa were respectively applied to the O-ring under uniform squeeze rate of 20%, the stresses of the O-ring under uniform squeeze rate were respectively analyzed in this paper.

The isochromatic fringe patterns of the O-ring under 20% squeeze rate and with each internal pressure were almost uniform with arbitrary position along the O-ring that is, without positions. Therefore the isochromatic fringe patterns of position I of the O-ring are shown in Fig. 3.

Isochromatic fringe patterns of the O-ring under uniform squeeze rate of 20% were changed according to the variations of internal pressures.

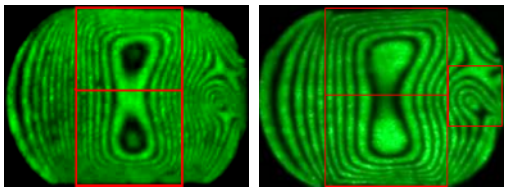

(a) P_i=0 (b) P_i=0.98MPa

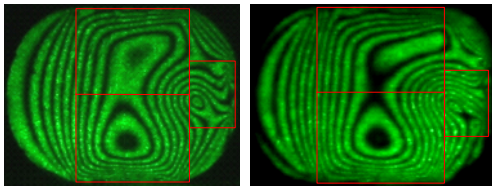

(c) P_i=1.96MPa (d) P_i=2.94MPa

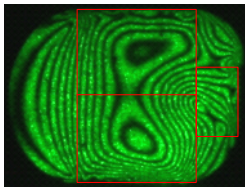

(e) P_i=3.92MPa

Fig. 3. Isochromatic fringe patterns of the stress frozen O-ring under 20% squeeze rate and under internal pressure.

An especially isochromatic fringe patterns in the right side of the O-ring is completely different according to the variations of the internal pressure.

But isochromatic fringe patterns in the left side of the O-ring under uniform squeeze rate are very similar to each other according to the variations of internal pressure.

Fig. 4. shows the regions in which photoelastic isochromatic data were measured.

Experimental data measured on the upper region (= Region 1), on the lower region (= Region 2) and on the front region (= Region 3) were respectively used to obtain the stress components of the three regions

Region ① in Fig. 4 is the duplicated region of Region 1 and Region 2. Region ② in Fig. 4 is the reiterated region of Region 1, Region 2 and Region 3. Experimental data measured in Region ① and Region ② were respectively used to connect the stress contours and isochromatic fringe patterns in region 1, region 2 and region 3 smoothly.

Fig(a) and Fig(b) in Fig. 5 are, respectively, the actual isochromatics in Region 1, Region 2 and Region 3, and the plotted isochromatics from the new photoelastic experimental hybrid method in Region 1,

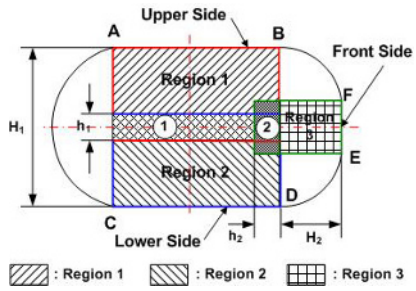

Fig. 4. The regions which photoelastic isochromatic data were measured.

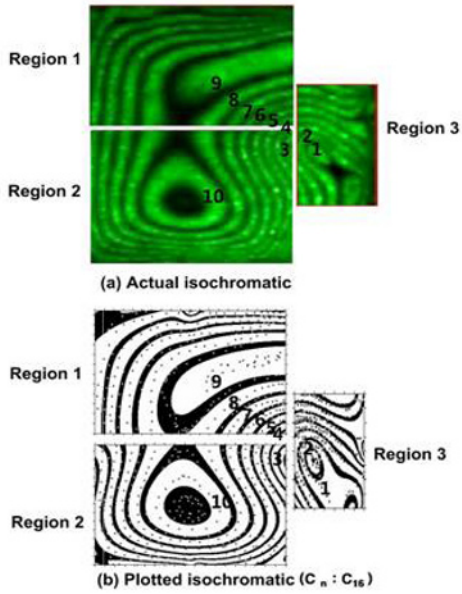

Fig. 5. Actual photoelastic fringe patterns and plotted photoelastic fringe patterns from the photoelastic experimental hybrid method (squeeze rate: 20%, pressure: 2.94 MPa).

Region 2 and Region 3 when the squeeze rate of O-ring is 20% and internal pressure applied to the O-ring is 2.94 MPa.

The "+" symbol in Fig. 5 indicates the measured position. All experimental data were measured on the centerline of each black band and each white band. As shown in Fig. 5, actual isochromatic fringe pattern is almost identical to the plotted isochromatic fringe pattern. All "+" symbols are located on the centerline of the black band and white band. These results mean that the new photoelastic experimental hybrid method developed in this research is effective.

In this research, contact stresses σ_x, σ_y and τ_{xy} and internal stresses σ_x, σ_y and τ_{xy} in the upper side, in the lower side and in the front side of the O-

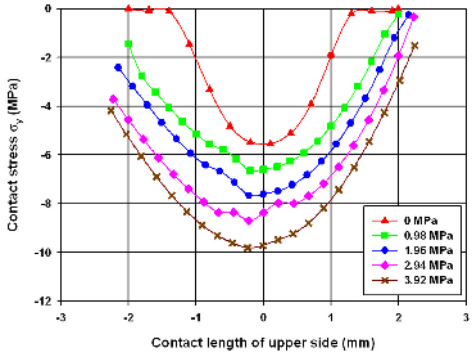

Fig. 6. Contact stress distributions σ_y of upper side of O-ring under 20% squeeze rate and internal pressure.

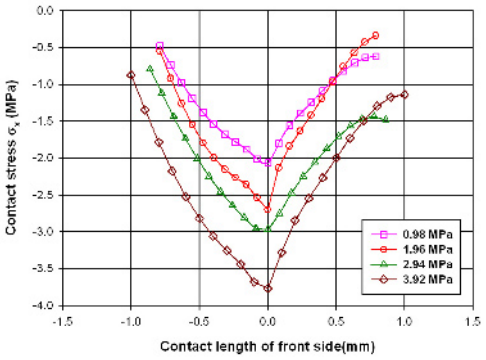

Fig. 7. Contact stress distribution σ_x of the front side of O-ring under squeeze rate of 20% and internal pressure.

ring under uniform squeeze rate of 20% were analyzed with the internal pressure.

Among them, the important contact stresses and internal stresses in each side were analyzed as follows:

Fig. 6 shows contact stress distributions σ_y of upper side of O-ring under 20% squeeze rate and internal pressure. The magnitudes of σ_x, σ_y and τ_{xy} are increased as the internal pressures increase. The distributions of σ_y and τ_{xy} are almost symmetric about the center of the contact line.

The positions of maximum σ_y move to the left side from the center of the contact line, that is, to the direction of applied internal pressure when the internal pressure is greater than 1.96 MPa. Positions at which maximum σ_y's occur are the center of the contact line when internal pressure is less than 1.96 MPa.

The stress distributions and maximum positions of the lower side of the O-ring with internal pressures are very similar to those of the upper side of the O-ring with internal pressures. The stress distributions of contact stress components σ_x, σ_y and τ_{xy} in the front side of the O-ring under squeeze rate of 20% and internal pressure are different from each other.

Among the stress components σ_x, σ_y and τ_{xy} in the front side of the O-ring under squeeze rate of 20% and internal pressure, the stress distributions of contact stress σ_x are shown in Fig. 7.

As shown in Fig. 7, the maximums of the contact stress σ_x of the front side of O-ring under squeeze rate of 20% and internal pressure occur at the center of the contact line. Their values are much greater than the maximums of the contact stress τ_{xy} of the front side of the O-ring and are much smaller than the maximums of the contact stress σ_y of the upper side of the O-ring.

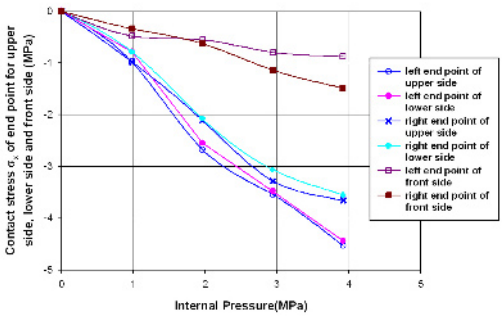

Fig. 8. Relationship between internal pressure and contact stress σ_x of end point for each side of O-ring under squeeze rate of 20%.

Fig. 8 shows the relationship between the internal pressure and contact stress σ_x of the end point for the upper side, lower side and front side of the O-ring under squeeze rate of 20%.

Symbols , , , , and etc, respectively, indicate the experimental data of contact stress σ_x of the left end point of the upper side and of the lower side(points A and C), of the right end point of the upper side and lower side(points B and D), left end point and right end point of the front side (points E and F) etc. Contact stress σ_x of the left end point of the upper side is slightly greater than the contact stress σ_x of the left end point of the lower side. Contact stress σ_x of the right end point of the upper side is slightly greater than the contact stress σ_x of the right end point of the lower side. Contact stress σ_x of the right end point of the front side is slightly greater than the contact stress σ_x of the left end point of the front side. Contact stress σ_x of the left end point of upper side or lower side is greater than the contact stress σ_x of the right end point of the upper side or lower side.

Contact stress σ_x of the right end point of the upper side or lower side is much greater than the contact stress σ_x of the left end point or right end point of the front side. Magnitudes and distributions in the contact stress σ_y of the end point for the upper side, lower side and front side are respectively very similar to those in the contact stress σ_x of the end point of the upper side, lower side and front side.

Fig. 9 is the relationship between internal pressure and maximum contact stress σ_y for upper side, lower side and front side of the O-ring under squeeze rate of 20%.

Fig. 10 show the relationship between internal pressure and maximum contact stress τ_{xy} for the upper side, lower side and front side of the O-ring under a squeeze rate of 20%.

Maximum contact stresses σ_y's of the upper side are very similar to those of the lower side. Maximum contact stress σ_y's of the front side are much less than those of the lower side. Maximum of the contact stress τ_{xy} of the upper side is identical to those of the lower.

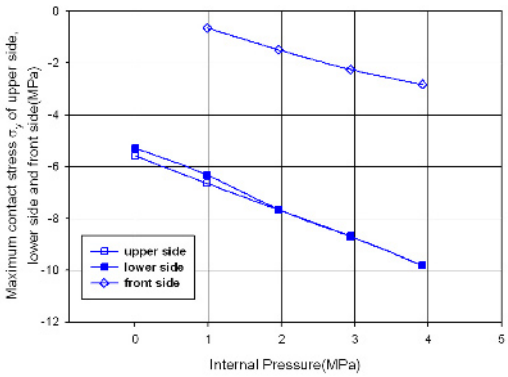

Fig. 9. Relationship between internal pressure and maximum contact stress σ_y in each side.

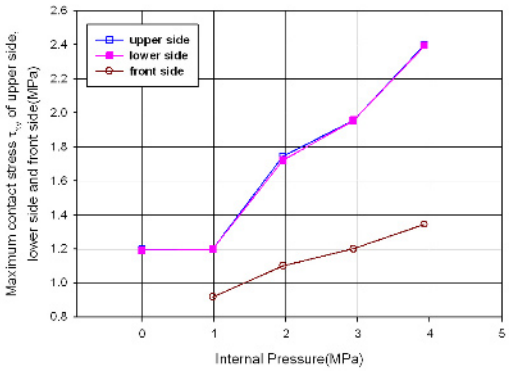

Fig. 10. Relationship between internal pressure and maximum contact stress τ_{xy} for each side of the O-ring under squeeze rate of 20%.

Fig. 11, Fig. 12 and Fig. 13, respectively, show the stress contour of σ_x / p_0, σ_y / p_0 and τ_{xy} / p_0 obtained from the new photoelastic experimental hybrid method for the O-ring under a squeeze rate of 20% and internal pressure.

As shown in Fig. 11, when the O-ring is only under uniform squeeze rate, that is, $p_i = 0$, distributions of σ_x are symmetric in the right side and in the left side about the center of the contact line. Distributions of σ_x in the upper region are almost identical to those of the lower region. When the O-ring is under a uniform squeeze rate of 20% and the internal pressures

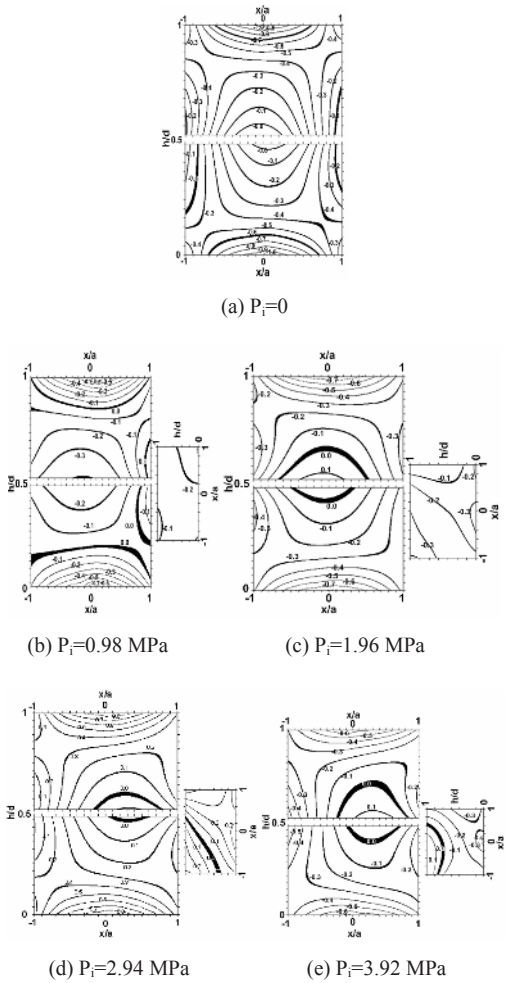

(a) P_i=0

(b) P_i=0.98 MPa (c) P_i=1.96 MPa

(d) P_i=2.94 MPa (e) P_i=3.92 MPa

Fig. 11. Stress contacts of σ_x / p_0 obtained from the new photoelastic experimental hybrid method for O-ring under squeeze rate of 20% and internal pressure.

are, respectively, 0.98 MPa, 1.96 MPa, 2.94 MPa or 3.92 MPa, and the stress distributions of σ_x are slightly unsymmetrical in the right side and in the left side about the center of the contact line. Distributions of σ_x in the upper region are different from those in the lower region. Magnitudes of σ_x in the front region slightly increase with a small increase of the internal pressure.

As shown is Fig. 12, when $p_i = 0$, the distributions of σ_y in the upper region are identical to those in the lower region. σ_y does not exist in the front region. When $p_i = 0.98 MPa$ or $p_i = 1.96 MPa$, the distribution of σ_y is slightly moved and twisted to the left side of the center contact line.

In the front region, (σ_y / p_0) 's occur. But they have a similar pattern respectively. When $p_i = 2.94$ MPa or $p_i = 3.92\ MPa$, the families of the high stress contour are moved and twisted slightly to the left side from the center of the contact line. When $p_i = 2.94\ MPa$, the stress contours of σ_y / p_0 in the front region have the same distribution as the previous distribution of σ_y / p_0. When $p_i = 3.92$ MPa, the magnitude of σ_y / p_0 is slightly greater than the magnitude of previous σ_y / p_0.

As shown in Fig. 13, when $p_i = 0$, the distributions of τ_{xy} / p_0 are symmetric to the right side and to the left side about the center of the contact line. Distribution patterns of τ_{xy} / p_0 in the upper region are identical to those in the lower region.

τ_{xy} / p_0 in the front region does not exist. When $p_i = 0.98\ MPa$, $p_i = 1.96\ MPa$, $p_i = 2.94\ MPa$ or $p_i = 3.92\ MPa$. Distribution patterns of τ_{xy} / p_0 in the upper region are almost identical to those in the lower region.

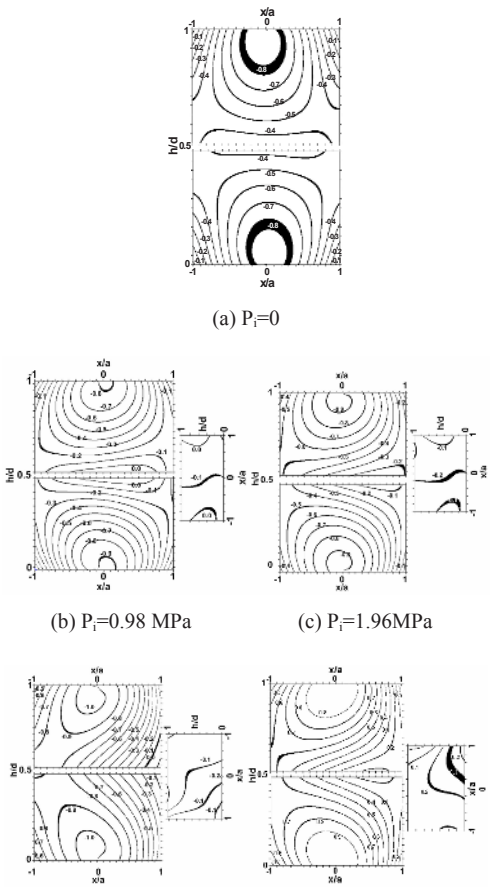

(a) P_i=0 (b) P_i=0.98 MPa (c) P_i=1.96MPa (d) P_i=2.94 MPa (e) P_i=3.92 MPa

Fig. 12. Stress contacts of σ_y / p_0 obtained from new photoelastic experimental hybrid method for O-ring under squeeze rate of 20% and internal pressure.

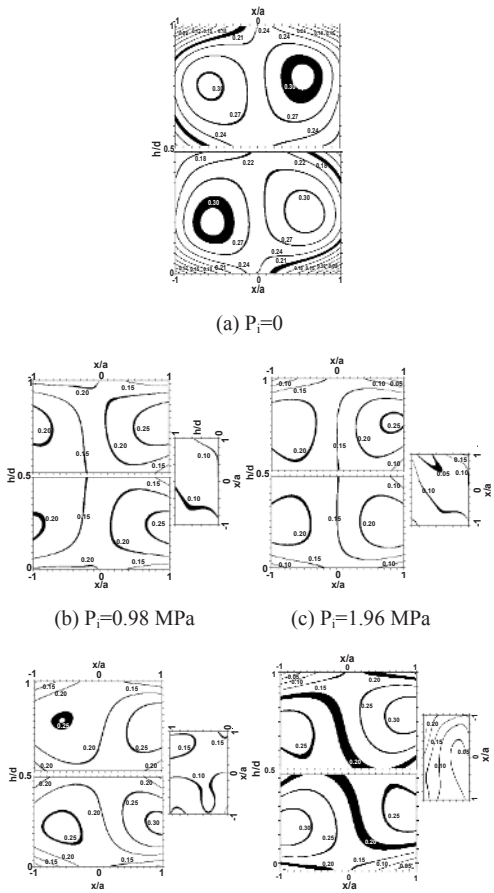

(a) P_i=0 (b) P_i=0.98 MPa (c) P_i=1.96 MPa (d) P_i=2.94 MPa (e) P_i=3.92 MPa

Fig. 13. Stress contours of τ_{xy} / p_0 obtained from the new photoelastic experimental hybrid method for O-ring under squeeze rate of 20% and internal pressure.

Magnitudes of τ_{xy}/p_0 in the upper region or the lower region increase gradually as the internal pressure increases until $p_i = 2.94\ MPa$.

When $p_i = 3.92\ MPa$, the magnitudes of τ_{xy}/p_0 become the greatest among all cases.

Magnitude of τ_{xy}/p_0 in the front region increases gradually as the internal pressure increases.

5. Conclusions

The following conclusions were obtained based on the experimental results and discussions for the case in which the uniform squeeze rate of the O-ring is 20% and internal pressures applied to the O-ring are 0.98 MPa, 1.96 MPa, 2.94 MPa, and 3.92 MPa.

The new photoelastic experimental hybrid method for contact problem without external traction free boundary condition or internal traction free boundary condition was developed. It was validated.

The new photoelastic experimental hybrid method for contact problem can be applied to the stress analysis of structure without traction free boundary condition using the relative equation between two stress functions.

Contact stresses and internal stresses of the O-ring under uniform squeeze rate (about 20%) and internal pressure were analyzed by the new photoelastic experimentalhybrid method for the contact problem.

When the O-ring was under squeeze rate of 20% and under internal pressure, the contact stress σ_x's of the right end point and the left end point on the upper side linearlyincreased as the internal pressure increased. When p_i=0 and p_i= 0.98 MPa, σ_x's of the right end point and the left end point on the upper side were ,respectively, 0 and 1 MPa. When the internal pressures were 1.96 MPa and 2.94 MPa, σ_x's values of the rightend point and the left end point on the upperside were slightly greater than the internal pressures. Absolute values of σ_x at the left end point were greater than those at the rightend point on the upper side. When the internal pressure was 3.92 MPa, the absolute value of σ_x at the left end point was slightly greater than the internal pressure, and the absolute value of σ_x at the right end point was slightly less than the internal pressure.

Absolute value maximums of σ_x on the upper side or on the lower side were between 6 MPa and 9MPa when the internal pressures were varied between 0 MPa and 3.92 MPa. Absolute value maximums of σ_y on the upper side or on the lower side were between 6 MPa and 10 MPa when the internal pressures were varied between 0 MPaand 3.92 MPa. Absolute value maximums of τ_{xy} were between 1.25 MPa and 2.4 MPa when the internal pressure was changed between 0 MPa and 3.92 MPa.

Absolute values of σ_x at the right end point at the left end point, on the upper side or lower side on the front side sharply increased as the internal pressures increased. Their values were greater than internal pressures when internal pressures are between 1.96 Mpa and 3.92 Mpa. Absolute values of σ_x on the left end point on the front side smoothly increased as the internal pressures increased.

Their values were less than the internal pressure values. The absolute maximum of σ_x onthe front side linearly varied with the magnitude of the internal pressure. Absolute values of σ_x on the front side were between 0.3 MPa and 1.3 MPa when internal pressures were 0.98 MPa and 3.92 MPa.

The distributions of σ_y and τ_{xy} are almost symmetric about the center of the contact line. The positions of maximum σ_y move to the left side from the center of the contact line, that is, in the direction of applied internal pressure when the internal pressure is greater than 1.96 MPa. Positions atwhich maximum σ_y's occurs are the center of the contact line when internal pressure is less than 1.96 MPa.

The maximums of the contact stress σ_x of the front side of O-ring under squeezerate of 20% and internal pressure occur at the center of the contact line. Their values are much greater than the maximums of the contact stress τ_{xy} of the front side of the O-ring and are much smaller than the maximums of the contact stress σ_y of the upper side of the O-ring.

Maximum contact stresses σ_y's of theupper side are very similar to those of the lower side. Maximum contact stress σ_y's of the front side are much less than those of the lower side. Maximums of the contact stress σ_x of the upper side, of lower side and of front side are respectively, very similar to the maximums of the contact stress σ_y of the upper side, of lower side and of front side. The maximum of the contact stress τ_{xy} of the upper side is identical to those of the lower.

When the O-ring is only under uniform squeeze rate, that is, $p_i = 0$, distributions of σ_x are symmetric on the right side and on the left side about the center of the contact line. Distributions of σ_x in the upper region are almost identical to those of the lower region, when the O-ring is under a uniform squeeze

rate of 20% and the internal pressures are, respectively, 0.98MPa, 1.96MPa, 2.94MPa or 3.92MPa, and the stress distributions of σ_x are slightly unsymmetrical in the right side and in the left side about the center of the contact line. Distributions of σ_x in the upper region are different from those in the lower region. Magnitudes of σ_x in the front region slightly increase with a small increase of the internal pressure.

When $p_i = 0$, the distributions of σ_y in the upper region are identical to those in the lower region. σ_y does not exist in the front region. When $p_i = 0.98MPa$ or $p_i = 1.96MPa$, the distributions of σ_y is slightly moved and twisted to the left side ofthe center contact line. In the front region, (σ_y / p_0) 's occur. But they have a similar pattern respectively. When $p_i = 2.94\ MPa$ or $p_i = 3.92\ MPa$, the families of the high stresscontour are moved and twisted slightly to theleft side from the center of the contact line. When $p_i = 2.94\ MPa$, the stress contours of σ_y / p_0 in the front region have the same distribution as the previous distribution of σ_y / p_0. When $p_i = 3.92\ MPa$, the magnitude of σ_y / p_0 is slightly greater than the magnitude of previous σ_y / p_0.

When $p_i = 0$, distributions of τ_{xy} / p_0 are symmetric to the right side and to the left side about the center of the contact line. Distributions patterns of τ_{xy} / p_0 in the upper region are identical to those in the lower region. τ_{xy} / p_0 in the front region does not exist. When $p_i = 0.98\ MPa$, $p_i = 1.96\ MPa$, $p_i = 2.94\ MPa$ or $p_i = 3.92\ MPa$. Distribution patterns of τ_{xy} / p_0 in the upper region are almost identical to those in the lower region. Magnitudes of τ_{xy} / p_0 in the upper region orthe lower region increase gradually as the internal pressure increases until $p_i = 2.94\ MPa$. When $p_i = 3.92\ MPa$, the magnitudes of τ_{xy} / p_0 become the greatest among all cases. Magnitude of τ_{xy} / p_0 in the front region increases gradually as the internal pressure increases.

Acknowledgment

This research was supported by Yeungnam University research grants in 2007.

References

[1] A. Strozzi, Static Stresses in an Unpressurized, Rounded, Rectangular, Elastomeric Seal, Asle Transactions, 29(4)(1986) 558-564.

[2] A. F George, A. Strozzi and J. I. Rich, Stress Fields in a Compressed Unconstrained Elastomeric O-ring Seal and a Comparison of Computer Predictions with Experimental Results, Tribol. Int., 20(1987) 237-247.

[3] E. Dragoni and A. Strozzi,Theoretical Analysis of an Unpressurized Elastomeric O-Ring Seal into a Rectangular Groove, Elsevier Sequoia, Wear, 130 (1989) 41-51.

[4] E. Dragoni and A. Strozzi, Analysis of an Unpressurized, Laterally Restrained, Elastomeric O-Ring Seal, Journal of Tribology, 110(1988) 193-200.

[5] A. Karaszkiewicz, Geometry and Contact Pressure of an O-Ring Mounted in a Seal Groove, Ind. Eng. Chem. Res. 29, (1990) 2134-2137.

[6] Il Kwon Lee, Chung Kyun Kim, Numerical Simulations on the O-ring Extrusion in Automotive Engines, Journal of Korean Society of Tribologists & Lubrication Engineers, 15(4)(1999) 297-303.

[7] Jeonghwan Nam, Jaisug Hawong, Osung Kwon, Songling Han, Gun Kwon, A Study on the Analysis of Contact Stress of O-Ring under Uniform Squeeze Rate by Photoelastic Experimental Hybrid Method, ATEM'07 OS16-2-4.

[8] J. S. Hawong, C. H. Lin, S. T. Lin, J. Rhee and R. E. Rowlands, A Hybrid Method to Determine Individual Stresses in Orthotropic Composites Using Only Measured Isochromatic Data, Journal of Composite Material, 29(18)(1995) 2366-2387.

[9] D. C. Shin, J. S. Hawong, H. J. Lee, J. H. Nam and O. S. Kwon, Application of Transparent Photoelastic Experimental Hybrid Method to the Fracture Mechanics of Isotropic Material, Transactions of the Korean society of Mechanical Engineers(A), 22(5) 834-842.

[10] D. C. Shin, J. S. Hawong, J. H. Nam, H. J. Lee and O. S. Kwon, Application of Transparent Photoelastic Experimental Hybrid Method for the Fracture Mechanics of Orthotropic Material, Transactions of the Korean Society of Mechanical Engineers(A), 22(6)(1998) 1036-1044.

[11] J. S. Hawong, D. C. Shin and H. J. Lee, Photoelastic Experimental Hybrid Method for Fracture Mechanics of Anisotropic Materials"_ Experimental Mechanics, 41(1)(2001) 92-99.

[12] Dong-chul Shin, Jai-sug Hawong and Jong-Hyun Sung, Development of Dynamic Photoelastic Experimental Hybrid Method for Propagating Cracks in Orthotropic Material, Transactions of Korean Society of Mechanical Engineers A, 27(8)(2003)

1273-1280.
[13] Dong-chul Shin, Jai-sug Hawong and Sung-su Nam, Application of the static Photoelastic Experimental Hybirid Method of the Crack Propagating Criterion for Isotropic Materials Transactions of Korean Society of Mechanical Engineers A, 28 (8) (2004) 1229-1236.
[14] N. I. Muskhelishvili, Some Basic Problems of Mathematical Theory of Elasticity, 4th Edition, P.Noordhoff Ltd., Groningen Netherlands, (1963).
[15] A. C. Ugural, S. K. Fenster, Advanced Strength and Applied Elasticity Elsevier, (1981) 70.
[16] D. A. Hills, D. Nowell and A. Sackfield, Me chanics of Elastic Contacts.
[17] R. C. Sampson, A Stress-Optic Law for Photoelastic Analysis of Orthotropic Composites"_ *Experimental Mechanics*, (1970) 210-216.
[18] J. S. Hawong, J. H. Nam, S. L. Han and S. H. Park, Contact stress of O-ring under uniform squeeze rate by photoelastic experimental hybrid method"_Journal of Mechanical Science and Technology 22, (2008) 2337-2349.
[19] M. S. Bazaraa and C. M. Shetty, Nonlinear Programming : theory and algorithms, John Wiley & Sons Inc, (1979).

Jai-Sug Hawong received a B.S. degree in Mechanical Engineering from Yeungnam University in 1974. Then he received his M.S. degree and Ph.D. degree from Yeungnam University in Korea in 1976 and from Kanto Gakuin University in Japan in 1990, respectively. Prof. Hawong is currently a professor at the school of Mechanical Engineering at Yeungnam University, in Gyeongsan city, Korea. He is currently serving as an vise-president of Korea Society Mechanical Engineering.
Prof. Hawong's research interests are the areas of static and dynamic fracture mechanics, stress analysis, experimental mechanics for stress analysis and composite material etc.